Characterization of Reversible Associations by Sedimentation Velocity with UltraScan

Borries Demeler,* Emre Brookes, Renjing Wang, Virgil Schirf, Chongwoo A. Kim

We compare here the utility of sedimentation velocity (SV) to sedimentation equilibrium (SE) analysis for the characterization of reversible systems. Genetic algorithm optimization in UltraScan is used to optimize the model and to obtain solution properties of all components present in the system. We apply our method to synthetic and experimental data, and suggest limits for the accessible kinetic range. We conclude that equilibrium constants obtained from SV and SE analysis are equivalent, but that SV experiments provide better confidence for the K_d, can better account for the presence of contaminants and provide additional information including rate constants and shape parameters.

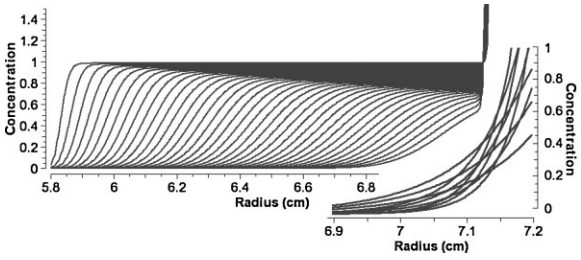

Introduction

Analytical ultracentrifugation has long been accepted as the gold standard for the characterization of macromolecular properties as well as the properties of reversible and irreversible reactions among macromolecules in the solution phase. The ability to work in the solution phase permits the investigator to modulate macromolecular concentration, concentration of ligands, buffer conditions such as pH, ionic strength, and oxidation state, as well as the temperature of the reaction, and to closely match physiological conditions.

Two principle experiments are generally performed in the analytical ultracentrifuge, sedimentation velocity (SV), and sedimentation equilibrium (SE). SV experiments are performed at higher speed, and observe the macromolecular sedimentation and diffusion transport by monitoring the concentration profiles of all solutes present in the solution over time. SE experiments monitor the equilibrium gradients obtained at the end of the SV experiment when all flow ceases and sedimentation and diffusion transport are exactly balanced.

In the SV experiment, the sedimentation and diffusional flow are inversely proportional to the frictional properties of the particle, and therefore shape information is also available. At hydrodynamic equilibrium all flow ceases and shape information cannot be obtained. Instead, the gradient obtained at equilibrium is an exponential function, whose exponent is proportional to the molecular weight of the solute. Each species present in the solution contributes its own gradient to the overall observed gradient, and the observed gradient is a superposition of exponentials (a review of first principles in sedimentation and diffusion can be found in van Holde).[1]

When interpreting such equilibrium gradients by curve fitting, all contributing exponentials need to be deconvoluted and each component's molecular weight and partial concentration should be resolved. However, this is an ill-conditioned problem, especially when fitting noisy data, limiting the resolution of this approach. When a reversible system is fitted, the relative proportion of each species along the concentration gradient changes according to mass action laws, and the ratios of the reacting species at each concentration point in the gradient are dependent on

B. Demeler, E. Brookes, R. Wang, V. Schirf, C. A. Kim
Department of Biochemistry, The University of Texas Health Science Center at San Antonio, 7703 Floyd Curl Drive, San Antonio, Texas 78229, USA
Fax: (+210) 567 6595; E-mail: demeler@biochem.uthscsa.edu

DOI: 10.1002/mabi.200900481

the equilibrium constant, which provides a convenient constraint for the data fit.

From a practical perspective, it is nearly impossible to distinguish reacting systems from non-interacting systems when only a single scan is considered. In fact, a non-interacting model generally produces lower residuals due to the absence of the equilibrium constraint and the availability of additional degrees of freedom in the model. An optimal experimental design for a reversibly associating system will therefore examine multiple loading concentrations ranging over a large concentration range and measure multiple speeds and fit all observations simultaneously, designating equilibrium constants and molecular weights as global parameters.

However, contributing contaminants are often difficult, if not impossible to detect by SE and can distort the obtained information. Hence, such measurements will always require very pure preparations, and SV or gel electrophoresis should be performed first to ascertain the purity of the system.

As in SE experiments, it is difficult to distinguish interacting from non-interacting systems in a single SV experiment. Radial dilution imposes a slight variation on the distribution of reacting species along the concentration gradient over the course of the SV experiment, but it is generally small enough so that even rapidly equilibrating systems can still be well approximated by non-interacting solutions. It is important to note that the apparent hydrodynamic species at each point in the concentration gradient is represented by the weight-average sedimentation coefficient and the gradient-average diffusion coefficient of all reacting species.[2,3] Rapidly interacting systems therefore produce continuous sedimentation coefficient distributions instead of showing discrete species reflecting individual components.

Attempts to extract equilibrium constants from rapidly interacting systems by fitting weight-average sedimentation coefficients observed in SV experiments to isotherms or to Lamm Equation solutions for rapidly self-associating models have been reported previously,[4] however, kinetic information was not considered in this approach. When the reaction rate is slow compared to the time scale of the SV experiment, the reacting species are separated before being able to re-equilibrate, and will indeed appear as discrete species analogous to a non-interacting system.[5,6] The relative amount of each species will depend on the loading concentration and equilibrium constant of the system. Hence, a reacting system can be clearly distinguished from a non-interacting system by two analysis results that are readily observed in a van Holde–Weischet integral distribution plot.[7] First, a change in the *s*-distribution with a change of loading concentration; second, the shape of the distribution is indicative of the reaction rate. Rapid kinetics will produce a smooth change in *s*, with a shape similar to the right half of a parabola, while slow kinetics or non-interacting systems will produce discrete separation between species (see Figure 1 and 2).

Recently, we have integrated a genetic algorithm optimization approach into UltraScan[8,9] for analyzing reversible systems by SV experiments. In this study we compare the results obtained from SV and SE experiments when fitting reversibly self-associating systems. We chose to demonstrate the reproducibility of our approach applied to SV analysis by analyzing two simulated monomer–dimer datasets which had realistic noise added that is similar to that observed in a well-tuned Beckman XL-A instrument. In such simulated data the performance of the optimization method can be ascertained, and the fitting results can be directly compared to the input parameters.

Secondly, we compared the SV results from an experimental system, the C-terminal domain of the human Polycomb Group protein RING1B (C-RING1B), with the results obtained from SE analysis in order to validate the methods against each other. C-RING1B possesses several characteristics which makes it suitable for our study. First, C-RING1B dimerizes weakly in solution [10,11] and its monomer–dimer equilibrium is in a concentration range well suited for our comparison studies. Second, there are several surface residues, both polar and apolar (K261A, V265E, and L269E),[12,13] that were available to mutate to affect the equilibrium constant of the dimerization.

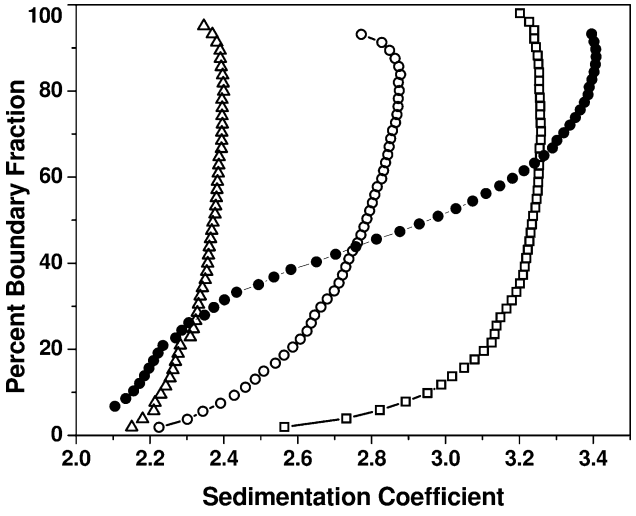

Figure 1. van Holde–Weischet integral distribution plots for a simulated monomer–dimer system (open symbols) at 0.1, 1, and 10 times the K_d concentration (open triangles, circles, and squares, respectively, for a fast association with a k_{off} rate of 1×10^{-3} s^{-1}), and a non-interacting equal mixture of monomer and dimer (filled circles). Fast reacting reversible systems form characteristic half-parabola shaped *s*-distributions that move to the right with increase in concentration due to the increased relative proportion of dimer, while distributions from non-interacting systems are invariant with concentration, and can show more discrete species.

Macromol. Biosci. **2010**, *10*, 775–782

Macromolecular Journals

DOI: 10.1002/mabi.200900481

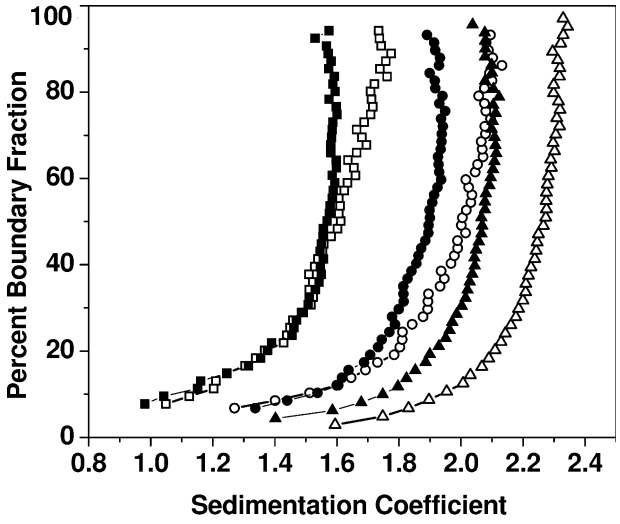

Figure 2. van Holde–Weischet integral distributions for C-RING1B wildtype (open symbols) and C-RING1B K261A mutant (filled symbols) at loading concentrations of 0.3 OD 230 nm (4.8×10^{-6} M, squares), 0.3 OD 280 nm (17.1×10^{-6} M, circles), and 0.9 OD 280 nm (51.2×10^{-6} M, triangles). Increasing loading concentrations cause a shift of the sedimentation coefficient distribution to the right for both species, and a characteristic half-parabola shape of the distributions are indicative of reversible self-association. Furthermore, the wildtype distributions are further shifted to the right than the mutant for all loading concentrations, indicating a lower K_d for the wildtype.

Experimental Part

Sedimentation Experiments

All sedimentation experiments were carried out in a Beckman XLI analytical ultracentrifuge at the Center for Analytical Ultracentrifugation of Macromolecular Assemblies at the University of Texas Health Science Center at San Antonio (UTHSCSA). All experiments were performed at 20 °C and diluted to the desired concentration with a 10×10^{-3} M sodium phosphate buffer, pH 7.0, containing 50×10^{-3} M NaCl and were scanned at either 230 or 280 nm. SV experiments were measured in intensity mode at 50 krpm in standard 2-channel centerpieces in an AN-50Ti rotor, and at two loading concentrations (0.3 and 0.9 OD, corresponding to 17.1 and 51.2×10^{-6} M, respectively) for both wildtype and mutants. SE experiments were measured in absorbance mode at three loading concentrations (0.3, 0.5, and 0.7 OD 280 nm) and at four speeds (30, 35, 40, and 50 krpm), until equilibrium was reached. Partial specific volumes were determined with UltraScan to be 0.730 ml · g^{-1} for RING1B and 0.729 ml · g^{-1} for RING1B-K261A.

Data Analysis

All data analysis was performed with UltraScan ver. 9.9.[8,9] SE experiments were evaluated with the global equilibrium fitting module of UltraScan. SV experiments were first fitted by two-dimensional spectrum analysis,[14,15] fitting time- and radially-invariant noise components as well as the meniscus position. Subsequently, the data were analyzed by the enhanced van Holde–Weischet analysis,[16] and overlays of integral distribution plots were used to compare sedimentation distributions. Next, wildtype and K261A data were fitted by genetic algorithm optimization[17] to the adaptive space-time finite element method (ASTFEM) solution of the Lamm Equation solution for reversible reactions.[18] 100 Monte Carlo iterations were used in each genetic algorithm fit to determine 95% confidence intervals for each parameter[19] and to confirm that all fitted parameters are well within the linear constraints of the genetic algorithm limits for each parameter and that no artificial pegging of the parameters to one of the constraint limits occurred.

During fitting of wildtype and K261A experimental data to reversible models, monomer molecular weights were kept fixed at the molecular weight derived from sequence (13.73 kDa for wild type, and 13.67 kDa for the K261A mutant). Simulated data were calculated for a monomer–dimer equilibrium at 60 krpm with a monomer molecular weight of 20 kDa, and frictional ratios of 1.25 for both monomer and dimer species, and a rate constant of 1×10^{-3} s^{-1}. For simulated data fits, all parameters were floated. The data were simulated with the same ASTFEM solution used above for fitting of experimental data, with 0.5% added random noise, which is equivalent to the noise typically observed in the Beckman absorbance system. Simulations were performed for three concentrations ranging from ten-fold below to ten-fold above the K_d concentration. For comparison, a non-interacting model with the same hydrodynamic parameters was simulated with the non-interacting ASTFEM solution.[20] All optimization computations were performed on the TeraGrid clusters Lonestar, Queenbee or Bigred, or on the Bioinformatics Core Facility clusters Laredo, Jacinto or Alamo at UTHSCSA.

Preparation of Mutant and Wildtype Protein

C-RING1B was cloned into a modified pET-3c vector which resulted in the translation of a polypeptide consisting of a MHHHHHHA-MENLYFQGTR leader sequence followed by human RING1B residues 222–336. All mutants were made using the QuickChange mutagenesis kit (Stratagene). All proteins were expressed in BL21-Gold (DE3) cells (Stratagene) that had been pre-transformed with the pRARE plasmid (Novagen). Typically, cells from one liter of bacterial culture were resuspended in 10 ml of 50×10^{-3} M tris pH 8.0, 100×10^{-3} M NaCl, 25×10^{-3} M imidazole pH 7.5, 1×10^{-3} M PMSF, and 5% glycerol, lysed by sonication, and extraction of the protein was carried out using Ni affinity chromatography, digestion with TEV to remove the leader sequence followed by anion exchange chromatography.

Results and Discussion

Kinetic Effect

First, we determined the relative signal strength of the kinetic rate constant. The kinetic effect in a velocity experiment can only be observed if the reaction rate is sufficiently slow compared to the speed of sedimentation.

Sedimentation speed depends both on rotor speed and on molecular weight and shape of a solute. In order to determine the limits of the reaction rates that can be measured in an ultracentrifuge, we have simulated the signal obtained for a range of molecular weights for globular proteins undergoing a monomer–dimer equilibrium, as a function of the reaction rate at the maximum speed of 60 krpm (the maximum speed possible in the Beckman Optima XL analytical ultracentrifuges). The monomer–dimer equilibrium was simulated with the ASTFEM solution,[18] assuming a frictional ratio of 1.25 for each species. To quantify the kinetic effect we simulated each species as an infinitely fast reaction using a k_{off} rate of 10 s^{-1}. We then compared this test function against a second simulation for an identical system, with only the rate constant changed to a lower value**.** The residual mean square deviation (RMSD) difference between the latter function and the test function was calculated using the least squares metric, and plotted for each molecular weight and rate constant in Figure 3.

All simulations were performed with 0.5% random noise. Differences in RMSD below this level will be lost in experimental noise. RMSD levels above this level should be detectable with a well-tuned instrument. The results are shown in Figure 3 and demonstrate the expected effect. The larger the molecule, the faster is the reaction rate that can be measured with SV. Consequently, a larger RMSD difference results in a higher confidence of the determined rate constant. The data shown in Figure 3 can be used to predict the range of fastest reaction rates accessible by SV as a function of molecular weight.

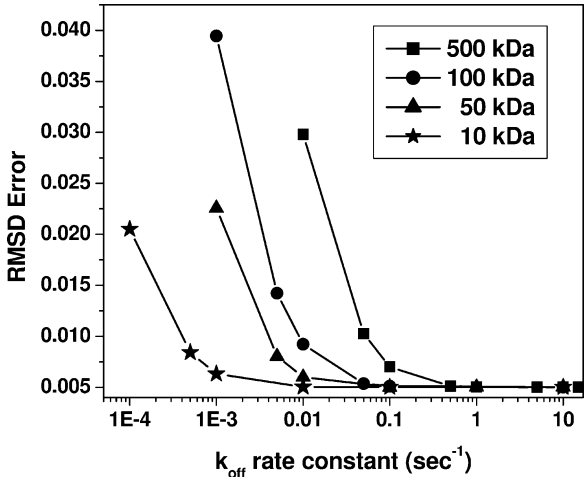

Figure 3. RMSD signal differences between a fast reacting system ($k_{off} = 10\ s^{-1}$) and indicated rate constants for different molecular weight species at 60 krpm. For each molecular weight, the fast reacting system is compared by the least squares metric with an identical system that differs only in the rate constant. All models are simulated with the ASTFEM[18] solution assuming a frictional ratio of 1.25, and include stochastic noise consistent with that observed in the XLA. The RMSD error represents a measure for the signal difference observed between the indicated rate constant and a system that reacts infinitely fast on the time scale of the velocity experiment. Due to the increased sedimentation rate for larger molecules, faster reaction rates can be detected more reliably from larger molecules, where signal differences are greater. The greater the RMSD error, the more reliable is the determination of the off-rate.

Simulated Monomer–Dimer System

The results of the simulated data are shown in Table 1, and a van Holde–Weischet integral distribution plot for all simulated concentrations is shown in Figure 1. These results demonstrate that our approach is able to reproduce all target values within the 95% confidence intervals determined by the Monte Carlo analysis. All parameters were reproduced within less than 3% error, except the equilibrium constant (10.44%), and the rate constant (46.60%). In light of the results shown in Figure 3, the higher error rate for the rate constant is expected. Even for a 60 krpm rotor speed, a 20 kDa sample does not produce a significant kinetic effect at a k_{off} rate of 0.001 s^{-1}, and hence the rate constant cannot be very reliably determined in this case, even though the result is well within the 95% confidence interval, which also correctly reflects the low confidence in this parameter determination.

In contrast, a second simulation at 60 krpm with a higher molecular weight monomer–dimer system (150 kDa, $f/f_0 = 1.25$ for both species) shows markedly improved errors and 95% confidence intervals, consistent with the data predicted in Figure 3. The results from this simulation are summarized in Table 2.

C-RING1B Results

Experimental data for the C-RING1B mutations V265E and L269E did not show any dimer formation and both SE and SV experiments were fitted well by single species models, producing the known monomer molecular weight. Integral van Holde–Weischet distributions showed a single species for all concentrations tested for these mutants, and the observed *s*-value distributions were consistent with a monomeric species (data not shown). Therefore, these mutants were not further considered for characterization by reversible monomer–dimer models.

However, both C-RING1B wildtype and the K261A mutation demonstrated significant dimerization potential and SE data could not be fitted well with a single species model. SE data were globally fitted first by a single species model, followed by a fixed molecular weight distribution model[8] and finally by a reversible monomer–dimer model. Fits to the fixed molecular weight distribution model resulted in molecular weight distributions ranging between 12 and 25 kDa, and RMSD values not significantly

Macromol. Biosci. **2010**, *10*, 775–782

Macromolecular Journals

DOI: 10.1002/mabi.200900481

Table 1. Genetic algorithm fitting results for the 20 kDa simulated monomer–dimer system containing 0.5% noise. All parameters were floated and 95% confidence intervals were determined by Monte Carlo analysis with 100 iterations.[19] All target parameter values were reproduced by the fit within the 95% confidence intervals. The equilibrium constant is given in arbitrary concentration units. Values in parentheses represent 95% confidence intervals.

Parameter	Fitted value	95% Confidence interval	Target value	% Error
Monomer *s* value	2.215×10^{-13} s	(2.166×10^{-13}, 2.263×10^{-13})	2.214×10^{-13} s	0.05
Monomer *D* value	9.596×10^{-7} cm$^2 \cdot$s^{-1}	(8.857×10^{-7}, 1.033×10^{-6})	9.595×10^{-7} cm$^2 \cdot$s^{-1}	0.01
Monomer mol. weight	1.996e + 04 Da	(1.863e + 04, 2.129e + 04)	2.000e + 04 Da	0.20
Monomer f/f_0	1.250E + 00	(1.179e + 00, 1.321e + 00)	1.250E + 00	
Dimer *s* value	3.578×10^{-13} s	(3.461×10^{-13}, 3.696×10^{-13})	3.515×10^{-13} s	1.79
Dimer *D* value	7.754×10^{-7} cm$^2 \cdot$s^{-1}	(7.363×10^{-7}, 8.144×10^{-7})	7.616×10^{-7} cm$^2 \cdot$s^{-1}	1.81
Dimer mol. weight	3.992e + 04 Da	(3.725e + 04, 4.259e + 04)	4.000e + 04 Da	0.20
Dimer f/f_0	1.221E + 00	(1.190e + 00, 1.252e + 00)	1.250E + 00	2.37
Equilibrium constant	9.055E–01	(6.962×10^{-1}, 1.115e + 00)	1.000E + 00	10.44
k_{off} rate constant	1.466×10^{-03} s^{-1}	(8.591×10^{-4}, 2.072×10^{-03})	1.000×10^{-03} s^{-1}	46.60

lower than RMSD values obtained from fitting to the more constrained reversible monomer–dimer model, which produced lower RMSD values for both wildtype and K261A than the single species model.

Single species models produced molecular weights that were between the known monomer and dimer molecular weights, with the wildtype showing a slightly higher single species molecular weight, consistent with the roughly twice higher K_d for K261A. All SE data analysis results are summarized in Table 3.

Sedimentation velocity (SV) data of wildtype and K261A exhibited all expected characteristics of a reversible monomer–dimer systems when analyzed by the enhanced van Holde–Weischet analysis (see Figure 2). The integral distribution plots showed a clear shift to higher *s* values for both wildtype and K261A with increasing loading concentration. Also, for both loading concentrations K261A showed a distribution shifted to lower sedimentation coefficients when compared to wildtype, indicating a reduced dimerization potential for K261A. When fitted by reversible monomer–dimer equilibrium models, all samples showed excellent fits with RMSD values between 3.7×10^{-3}–3.9×10^{-3} for 0.3 OD samples, and 6.0×10^{-3}–6.5×10^{-3} for 0.9 OD samples, nearly identical to the RMSD values observed in the more degenerate non-interacting models.

It should be noted that the RMSD for the K261A sample at high concentration was higher than typical (6.5×10^{-3}),

Table 2. Genetic algorithm fitting results for the 150 kDa simulated monomer–dimer system containing 0.5% noise. All run settings and analysis parameters were identical to conditions used for the fit shown in Table 1. All target parameter values were reproduced by the fit within the 95% confidence intervals. The equilibrium constant is given in arbitrary concentration units. Values in parentheses represent 95% confidence intervals. Due to the larger molecular weight, all parameters are better resolved than in the 20 kDa simulation, and errors are less than 1%.

Parameter	Fitted value	95% Confidence interval	Target value	% Error
Monomer *s* value	8.483×10^{-13} s	(8.473×10^{-13}, 8.494×10^{-13})	8.485×10^{-13} s	0.01
Monomer *D* value	4.893×10^{-07} cm$^2 \cdot$s^{-1}	(4.770×10^{-07}, 5.018×10^{-07})	4.902×10^{-07} cm$^2 \cdot$s^{-1}	0.02
Monomer mol. weight	1.501e + 05 Da	(1.460e + 05, 1.541e + 05)	1.500e + 05 Da	<0.01
Monomer f/f_0	1.250E + 00	(1.226e + 00, 1.274e + 00)	1.250e + 00	
Dimer *s* value	1.346×10^{-12} s	(1.343×10^{-12}, 1.350×10^{-12})	1.347×10^{-12} s	0.01
Dimer *D* value	3.883×10^{-07} cm$^2 \cdot$s^{-1}	(3.791×10^{-07}, 3.975×10^{-07})	3.891×10^{-7} cm$^2 \cdot$s^{-1}	0.02
Dimer mol. weight	3.001e + 05 Da	(2.921e + 05, 3.081e + 05)	3.000e + 05 Da	<0.01
Dimer f/f_0	1.250e + 00	(1.229e + 00, 1.272e + 00)	1.250e + 00	
Equilibrium constant	1.001e + 00	(9.888×10^{-01}, 1.013e + 00)	1.000e + 00	<0.01
k_{off} rate constant	1.001e–03 s^{-1}	(9.704×10^{-04}, 1.032×10^{-03})	1.000×10^{-03} s^{-1}	<0.01

Table 3. Sedimentation equilibrium (SE) fitting results for single species and reversible monomer–dimer models, as well as a fixed molecular weight distribution model with 100 species ranging between 1 and 50 kDa. Values in parentheses represent 95% confidence intervals. The results for the SV experiments are shown for comparison.

Fitting model	K261A	Wildtype
1-species MW	1.898×10^4 Da	1.909×10^4 Da
1-species RMSD	7.05×10^{-3}	9.48×10^{-3}
Fixed MW dist. RMSD	4.46×10^{-3}	4.26×10^{-3}
1-2 reversible RMSD	5.56×10^{-3}	5.41×10^{-3}
1-2 reversible K_d	54.0×10^{-6} M (29.1, 166.1)	22.7×10^{-6} M (8.64, 63.0)
Velocity results for comparison		
SV 0.3 OD_{280}	17.1×10^{-6} M (15.9, 18.4)	10.4×10^{-6} M (9.62, 11.4)
SV 0.9 OD_{280}	28.5×10^{-6} M (25.8, 31.8)	17.6×10^{-6} M (14.8, 21.6)

with the residuals for both non-interacting and reversible models showing a slight systematic deviation from the mean typical for samples that were not properly aligned in the rotor, causing convective effects.[21] A trace amount of a contaminant was apparent in all samples when analyzed with either the two-dimensional spectrum analysis or the genetic algorithm analysis when using non-interacting models, and therefore a non-interacting species was also included in the monomer–dimer fitting model to characterize this contaminant, which reduced the RMSD of the fit by approximately 2×10^{-3}. This contaminant could not be discriminated by SE, but may have biased the results from the SE data analysis.

The results for the SV experiments are summarized in Table 4 for both wildtype and K261A for both loading concentrations that were fitted. The results from both SV and SE experiments suggest that the K_d for wildtype is lower than for mutant K261A. Furthermore, the K_d values obtained from both SV and SE agreed well, and showed the same trend for wildtype versus mutant. While the K_d from SE experiments was generally slightly higher, the 95% confidence intervals obtained from SE data were much larger than those obtained from SV, but the 95% confidence interval from SE included the values obtained by SV analysis of both concentrations with the exception of the 0.3 OD K261A mutant sample, whose K_d was slightly lower than the 95% confidence interval obtained by equilibrium analysis.

We also noted a small but significant difference in the K_d for the two concentrations measured. The same trend of a lower K_d at the lower concentration was apparent in wildtype and mutant (7×10^{-6} M for wildtype and 11×10^{-6} M for K261A). It is not clear what causes this difference. We suggest that residual concentrations of purification- or storage buffer may play a role when samples were diluted with different amounts of running buffer. Another possibility is a concentration-dependent non-ideality effect.

The frictional ratio for the dimer of both samples appeared to be consistent for both concentrations, and also suggested a slightly more extended structure for both dimers. The frictional ratio for the K261A dimer was slightly higher than for the wildtype in both concentrations, possibly due to a de-stabilizing effect of the mutation.

Table 4. Sedimentation velocity (SV) fitting results for C-RING1B wildtype and K261A mutant to a reversible monomer–dimer equilibrium model that allows for the presence of a contaminant. Values in parentheses represent 95% confidence intervals.

Parameter	Wildtype, 0.3 OD	Wildtype, 0.9 OD	K261A, 0.3 OD	K261A, 0.9 OD
K_d ($\times 10^{-6}$ M)	10.4 (9.62, 11.4)	17.6 (14.8, 21.6)	17.1 (15.9, 18.4)	28.5 (25.8, 31.8)
k_{off} ($\times 10^{-5}$ s^{-1})	72.7 (26.5, 118.9)	84.3 (48.6, 120.0)	84.0 (46.4, 121.6)	14.1 (8.1, 20.1)
f/f_0 (monomer)	1.31 (1.28, 1.34)	1.14 (1.09, 1.19)	1.33 (1.32, 1.35)	1.19 (1.17, 1.21)
f/f_0 (dimer)	1.35 (1.33, 1.37)	1.31 (1.30,1.32)	1.43 (1.42, 1.45)	1.44 (1.43, 1.45)
f/f_0 (contaminant)	1.23 (1.18, 1.27)	1.24 (1.18, 1.3)	1.17 (1.12, 1.21)	1.49 (1.47, 1.56)
Contam. OD ($\times 0.01$)	3.49 (3.41, 3.57)	3.56 (3.37, 3.75)	3.35 (3.27, 3.44)	2.77 (2.58, 2.96)
Contaminant mol. wt. ($\times 1\,000$)	1.84 (1.71, 1.97)	2.33 (2.09, 2.56)	1.71 (1.59, 1.82)	3.00 (2.93, 3.06)

Macromol. Biosci. **2010**, *10*, 775–782

Macromolecular Journals
DOI: 10.1002/mabi.200900481

The frictional ratio of the monomer showed a similar consistent dependence on concentration as did the K_d, but in all cases the frictional ratio was lower for the monomer than the dimer. This compares favorably with the UltraScan Solution Modeler (US-SOMO) results.[22,23] Modeling the C-RING1B monomer (using the coordinates of a single C-RING1B chain from the C-RING1B/cbx7 cbox complex crystal structure[13] and dimer (using just the C-RING1B homodimer coordinates from the same structure) results in frictional ratios of 1.26 for the monomer and 1.32 for the wildtype dimer.

One outlier was apparent in the k_{off} value. While the k_{off} value for all measurements was pegged at the limit of the detection capability according to Figure 3, the value for the higher concentration of the K261A mutant indicated an approximately six-fold slower rate constant than the measurement for the lower concentration. We feel this result may be artifactual and due to the observed convection in the experiment. The rapid reaction rate is also consistent with the enhanced van Holde–Weischet results, which also suggest a rapid reaction (see Figure 2). We also attempted to float the monomer molecular weight parameter (data not shown), but the results suggested that the system became overdetermined, and no additional information could be extracted without also increasing the 95% confidence intervals.

Conclusion

Our results suggest that SV experiments can be used to determine equilibrium constants with higher confidence than is possible with SE, and produce equivalent RMSD values compared to those obtained by fitting with more degenerate non-interacting models. Furthermore, due to the improved separation capabilities of SV experiments, contaminants can be modeled without affecting the confidence of the reaction parameters, improving the data analysis resolution. Another important advantage of SV analysis is the ability to define shape parameters for all reacting species, as well as the kinetic rate constant, if the reaction rate is on the same time scale as the velocity experiment, or slower. The maximum rate constant that can be determined with SV is dependent on the maximum rotor speed and the molecular weight and shape of the solutes to be measured.

Genetic algorithm optimization for UltraScan is implemented on TeraGrid supercomputers to provide the ability to perform a simultaneous Monte Carlo analysis, which is helpful in order to ascertain the correct linear ranges of all parameters floated during the fit and to determine 95% confidence intervals. Since SV data analysis is computationally more demanding than SE analysis, the UltraScan software provides the ability to submit multiple simultaneous compute jobs via the TeraGrid Science Gateway portal[24] which provides considerable time savings and does not block the investigator's workstation with lengthy calculations.

We also noticed that the results were very sensitive to experimental noise and cell misalignments, therefore it is critically important that all noise contributions are minimized and optimal instrument performance is required. Our results suggest that SV data are preferable over SE data for modeling of reacting systems containing 2–3 components and provide improved confidence intervals and additional shape and kinetic information. For C-RING1B, the results suggest that mutations in positions 265 and 269 to charged side chains disrupt dimerization, and K261A was the only mutation that retained some of the dimerization potential seen in the wildtype, albeit with an increased K_d. All of these residues are in the coil–coil dimer interface region which is generally hydrophobic and explains the dimer destabilization effect.

We expect that additional information can be obtained from globally fitting SV experiments with multiple concentrations ranging over a 50–100-fold concentration range, centered on the K_d concentration. Such global analyses will show similar benefits as are obtained when multiple speeds and concentrations are fitted in SE experiments, and we plan to implement this capability in the next version of UltraScan. For single concentration fits, the best results will be obtained if sufficient signal from all represented species is available. The best signal from all oligomers will be observed close to the K_d concentration, where the RING1B results were measured and the simulated monomer–dimer systems were analyzed. The results from the 150 kDa monomer–dimer simulation, when compared to the 20 kDa monomer–dimer system, suggest that systems with higher molecular weights can provide a higher resolution for rate constants and even equilibrium constants. This result is consistent with the results shown in Figure 3, which also states that higher molecular weights produce a better signal for the rate constant. We therefore recommend that the highest possible speed is used for the measurement of reacting systems when quantitative information about K_d and rate constant are desired.

Acknowledgements: The development of the UltraScan software is supported by the *National Institutes of Health* through grant RR022200 (to BD). Supercomputer time allocations were provided through *National Science Foundation* grant TG-MCB070038 (to BD). CAK is supported by the *American Heart Association* (0830111N), the *American Cancer Society* (RSG-08-285-01-GMC) and the *Department of Defense Breast Cancer Research Program* (BC075278). We acknowledge the superb support provided by the *TeraGrid staff* at the Texas Advanced Computing Center at the University of Texas at Austin, and by *Jeremy Mann* at the Bioinformatics Core Facility at the University of Texas Health Science Center at San Antonio.

Received: December 31, 2009; Revised: February 10, 2010; Published online: May 18, 2010; DOI: 10.1002/mabi.200900481

Keywords: analytical ultracentrifugation; monomers; reversible associations; equilibrium complexes and rate constants; RING1B; polycomb repression complex 1; sedimentation velocity; structure; ultrascan

[1] K. E. van Holde, *Biophysical Chemistry*, 2nd edition, Prentice Hall, Englewood Cliffs, NJ 1985, Ch. 4, 5.
[2] J.-M. Claverie, H. Dreux, R. Cohen, *Biopolymers* **1975**, *14*, 1685.
[3] G. P. Todd, R. H. Haschemeyer, *Proc. Natl. Acad. Sci. U. S. A.* **1981**, *78*, 6739.
[4] P. Schuck, *Anal. Biochem.* **2003**, *320*, 104.
[5] J. R. Cann, D. C. Oates, *Biochemistry* **1973**, *12*, 1112.
[6] J. R. Cann, *Methods Enzymol.* **1978**, *48*, 248.
[7] B. Demeler, H. Saber, J. C. Hansen, *Biophys. J.* **1997**, *72*, 397.
[8] B. Demeler, UltraScan: "A Comprehensive Data Analysis Software Package for Analytical Ultracentrifugation Experiments", in: *Modern Analytical Ultracentrifugation: Techniques and Methods*, Royal Society of Chemistry, UK 2005, pp. 210–229.
[9] B. Demeler, *UltraScan ver. 9.9, release 1016*, The University of Texas Health Science Center, Dept. of Biochemistry 2009, http://www.ultrascan.uthscsa.edu.
[10] A. Czypionka, O. R. de los Paños, M. G. Mateu, F. N. Barrera, E. Hurtado-Gómez, J. Gómez, M. Vidal, J. L. Neira, *Biochemistry* **2007**, *46*, 12764.
[11] R. Wang, U. Ilangovan, A. K. Robinson, V. Schirf, P. M. Schwarz, E. M. Lafer, B. Demeler, A. P. Hinck, C. A. Kim, *Biochemistry* **2008**, *47*, 8007.
[12] I. Bezsonova, J. R. Walker, J. P. Bacik, S. Duan, S. Dhe-Paganon, C. H. Arrowsmith, *Biochemistry* **2009**, *48*, 10542.
[13] R. Wang, A. B. Taylor, B. Z. Leal, L. V. Chadwell, U. Ilangovan, A. K. Robinson, V. Schirf, P. J. Hart, E. M. Lafer, B. Demeler, A. P. Hinck, D. G. McEwen, C. A. Kim, (submitted).
[14] E. Brookes, R. V. Boppana, B. Demeler, *Computing Large Sparse Multivariate Optimization Problems with an Application in Biophysics* Supercomputing '06, 2006, ACM 0-7695-2700 -0/06.
[15] E. Brookes, W. Cao, B. Demeler, *Eur. Biophys. J.* **2010**, *39*, 405.
[16] B. Demeler, K. E. van Holde, *Anal. Biochem.* **2004**, *335*, 279.
[17] E. Brookes, B. Demeler, Parsimonious Regularization using Genetic Algorithms Applied to the Analysis of Analytical Ultracentrifugation Experiments *GECCO Proceedings* 2007, ACM 978-1-59593-697-4/07/0007.
[18] W. Cao, B. Demeler, *Biophys. J.* **2008**, *95*, 54.
[19] B. Demeler, E. Brookes, *Colloid. Polym. Sci.* **2008**, *286*, 129.
[20] W. Cao, B. Demeler, *Biophys. J.* **2005**, *89*, 1589.
[21] K. K. Arthur, J. P. Gabrielson, B. S. Kendrick, M. R. Stoner, *J. Pharm. Sci.* **2009**, *10*, 3522.
[22] E. Brookes, B. Demeler, C. Rosano, M. Rocco, *Eur. Biophys. J.* **2010**, *39*, 423.
[23] E. Brookes, B. Demeler, M. Rocco, *Macromol. Biosci.* **2010**, this issue. DOI: 10.1002/mabi.200900474
[24] UltraScan TeraGrid Science Gateway Portal: http://www.teragrid.org/gateways/projects.php?id=77.

DOI: 10.1002/mabi.200900481